Cellular/Molecular

Neuronal Hyperactivity Recruits Microglial Processes via Neuronal NMDA Receptors and Microglial P2Y12 Receptors after Status Epilepticus

Ukpong B. Eyo, Jiyun Peng, Przemyslaw Swiatkowski, Aparna Mukherjee, Ashley Bispo, and Long-Jun Wu
Department of Cell Biology and Neuroscience, Rutgers University, Piscataway, New Jersey 08854

Microglia are highly dynamic immune cells of the CNS and their dynamism is proposed to be regulated by neuronal activities. However, the mechanisms underlying neuronal regulation of microglial dynamism have not been determined. Here, we found an increased number of microglial primary processes in the hippocampus during KA-induced seizure activity. Consistently, global glutamate induced robust microglial process extension toward neurons in both brain slices and in the intact brain *in vivo*. The mechanism of the glutamate-induced microglial process extension involves the activation of neuronal NMDA receptors, calcium influx, subsequent ATP release, and microglial response through P2Y12 receptors. Seizure-induced increases in microglial process numbers were also dependent on NMDA receptor activation. Finally, we found that P2Y12 KO mice exhibited reduced seizure-induced increases in microglial process numbers and worsened KA-induced seizure behaviors. Our results elucidate the molecular mechanisms underlying microglia–neuron communication that may be potentially neuroprotective in the epileptic brain.

Key words: **epilepsy; glutamate; microglia; NMDA receptor; P2Y12 receptor; process extension**

Introduction

Microglia are the principal resident immune cells of the CNS and research in recent years is providing increasing evidence for their communication with neurons (Ransohoff and Perry, 2009; Eyo and Wu, 2013; Schafer et al., 2013). During development, they clear apoptotic neurons (Marín-Teva et al., 2004), promote the survival of cortical neurons (Ueno et al., 2013), and prune synapses (Paolicelli et al., 2011; Schafer et al., 2012). In the mature CNS, microglia represent the most dynamic and morphologically plastic cells identified to date (Davalos et al., 2005; Nimmerjahn et al., 2005). With their stationary somata and exquisitely motile processes, they effectively survey the surrounding microenvironment making frequent contacts with neuronal elements (Wake et al., 2009; Tremblay et al., 2010). However, the detailed mechanisms guiding microglial processes in response to neuronal activity have not been elucidated.

Glutamate is the major excitatory neurotransmitter in the CNS and the extracellular glutamate concentration is maintained at low levels (Tzingounis and Wadiche, 2007). Conditions with a significant increase in extracellular glutamate lead to increases in neuronal activity such as during epilepsy (During and Spencer, 1993; Meurs et al., 2008), characterized by an occurrence of seizures resulting from neuronal hyperactivities (Fisher et al., 2005). In addition, microglial activation is characteristic of epileptic murine brains compared with nonepileptic ones (Drage et al., 2002; Shapiro et al., 2008). Moreover, human patients with intractable seizures revealed an 11-fold increase in microglial reactivity in the CA1 (Beach et al., 1995) suggesting that periods of intense neuronal activity alter microglial state. However, the immediate consequences imposed on microglia by global increases in neuronal activity as occurs during epilepsy in the mammalian brain have not been studied.

In the present study, we first observed that acute seizures significantly alter microglial morphologies in the hippocampus leading us to investigate the role of a global increase of glutamate on microglial dynamics. We then performed two-photon time-lapse imaging and observed significant microglial process extension toward neuronal elements within minutes after bath application of glutamate. Deciphering the mechanism indicated the requirement of neuronal NMDA receptors, calcium influx, purinergic signals, and microglial P2Y12 receptors for glutamate-induced microglial process extension. This neuronal NMDA receptor-dependent microglial process alteration was recapitulated in the epileptic brain. Moreover, P2Y12 KO mice lacking such extensions experienced worse seizures suggesting that microglial process extensions perform neuroprotective functions. Our results delineate a novel form of microglia–neuron communication through neuronal NMDA receptors and microglial P2Y12 receptors that are relevant during epilepsy.

Received Jan. 29, 2014; revised May 26, 2014; accepted June 27, 2014.

Author contributions: U.B.E. and L.-J.W. designed research; U.B.E., J.P., P.S., A.M., and A.B. performed research; L.-J.W. contributed unpublished reagents/analytic tools; U.B.E., J.P., and L.-J.W. analyzed data; U.B.E. and L.-J.W. wrote the paper.

This work is supported by the National Institutes of Health (R01NS088627), American Heart Association (11SDG7340011), and Michael J. Fox Foundation. We thank Dr. Michael E. Dailey (University of Iowa) for providing us with P2Y12 knock-out mice.

The authors declare no competing financial interests.

Correspondence should be addressed to Dr. Long-Jun Wu, Department of Cell Biology and Neuroscience, Rutgers University, 604 Allison Road, Piscataway, NJ 08854. E-mail: lwu@dls.rutgers.edu.

DOI:10.1523/JNEUROSCI.0416-14.2014

 0270-6474/14/3410528-13$15.00/0

Materials and Methods

Animals. Both male and female mice were used in accordance with institutional guidelines, as approved by the animal care and use committee at Rutgers University. Heterozygous GFP reporter mice ($CX3CR1^{GFP/+}$) expressing GFP under control of the fractalkine receptor (CX3CR1) promoter (Jung et al., 2000) and transgenic mice expressing YFP in a subset of pyramidal neurons under control of Thy1 promoter (Thy1-YFP) (Feng et al., 2000) were obtained from The Jackson Laboratory. P2Y12 KO mice were obtained from Dr. Michael Dailey at the University of Iowa.

Slice preparation. Freshly isolated hippocampal slices were prepared from 4-week-old mice. Briefly, mice were anesthetized and swiftly decapitated. Brains from decapitated mice were carefully removed and placed in ice-cold, oxygenated (95% O_2 and 5% CO_2) artificial CSF (ACSF) with the following composition (in mM): 124 NaCl, 25 $NaHCO_3$, 2.5 KCl, 1 KH_2PO_4, 2 $CaCl_2$, 2 $MgSO_4$, 10 glucose, and sucrose added to make 300–320 mOsmol. Coronal slices (300 μm) were prepared and transferred to a recovery chamber for 30 or more minutes with oxygenated ACSF with the same composition as above at room temperature before imaging or electrophysiological studies. For calcium-free experiments, $CaCl_2$ was simply omitted from the ACSF formulation.

Two-photon and calcium imaging. Experiments were conducted at room temperature with slices maintained in oxygenated ACSF with the same composition as above in a perfusion chamber at a flow rate of 2 ml/min. Microglia were typically imaged using a two-photon microscope (Scientifica) with a Ti:sapphire laser (Mai Tai; Spectra Physics) tuned to 900 nm (for GFP microglia and YFP neurons) or 800 nm (for Sytox orange) with a 40× water-immersion lens (0.8 NA; Olympus). Fluorescence was detected using two photomultiplier tubes in whole-field detection mode and a 565 nm dichroic mirror with 525/50 nm (green channel) and 620/60 nm (red channel) emission filters. To separate GFP and YFP in some experiments, a 509 nm dichroic mirror with 500/15 and 537/26 nm emission filters was used. The laser power was maintained at 25 mW or below. We observed that neurons within the first 50 μm of the slice were heavily injured as they took up Sytox, a DNA-binding dye that labels cells with compromised cell membranes. However, beginning at ~50 μm in the slice, Sytox uptake was rarely observed (data not shown). Cells that are labeled with Sytox at these depths are usually not neurons as they possess nuclei with crescent shapes and usually reside in blood vessels reminiscent of endothelial cells rather than neurons whose nuclei are rounder. Thus, we imaged microglia between 50 and 100 μm where neurons maintained intact membranes without Sytox uptake.

For *in vivo* imaging, a small cranial window was made in the somatosensory cortex of adult 1- to 2-month-old mice. Microglia were imaged between 50 and 100 μm of the cortical surface, which typically resides in layer I of the cortex with dendrites (Kuhn et al., 2008), to ensure that glutamate was sufficiently delivered at such depths. Images were collected for at least 20 min to establish a baseline in normal ACSF and this was replaced with glutamate-containing ACSF and the same microglia were imaged for several minutes. Typically, 15 consecutive *z*-stack images were collected at 3 μm intervals every minute for slices and 30 consecutive *z*-stack images were collected at 1 μm intervals every 90 s for *in vivo* imaging.

To perform a general laser injury, we focused the laser 66× and parked it at ~250 mW at 900 nm for 3 s. To ablate single neurons, the laser was focused 100× at the center of the selected neuron and parked at ~400 mW at 900 nm for 1 s. Pilot experiments were performed on YFP-labeled neurons to confirm that injured neurons lose YFP expression immediately after the laser ablation. Experiments were performed with Sytox-containing media to confirm that only single neurons are labeled by the procedure.

For calcium imaging, Oregon Green BAPTA (OGB) at 0.5 mM was delivered locally to the hippocampal CA1 area through a glass pipette at 10 psi for at least 30 s. Cells were allowed to take up the dye and imaging commenced after at least 30 min.

Slice electrophysiology. Whole-cell patch-clamp recordings were made on the somata of CA1 pyramidal neurons or GFP-labeled microglia. Recording electrodes (4–5 MΩ) contained a K-based internal solution composed of the following (in mM): 120 K-gluconate, 5 NaCl, 1 $MgCl_2$, 0.5 EGTA, 2 MgATP, 0.1 Na_3GTP, and 10 HEPES, pH 7.2 (280 –300 mOsmol). Unless otherwise stated, the membrane potential was held at −60 mV for neurons and −20 mV for microglia (Boucsein et al., 2000; Wu et al., 2007; Wu and Zhuo, 2008) throughout all experiments. Data were amplified and filtered at 2 kHz by a patch-clamp amplifier (Multiclamp 700B), digitalized (Digidata 1440A), stored, and analyzed by pClamp (Molecular Devices). Data were discarded when the input resistance changed >20% during recording.

Epilepsy model. The 4- to 6-week-old heterozygous GFP reporter mice ($CX3CR1^{GFP/+}$) were intraperitoneally or intracerebroventricularly injected with KA at 18–22 mg/kg or 0.12–0.18 μg in 5 μl of ACSF, respectively. Seizure behavior was monitored under a modified Racine scale as follows: (1) freezing behavior; (2) rigid posture with raised tail; (3) continuous head bobbing and forepaws shaking; (4) rearing, falling, and jumping; (5) continuous level 4; and (6) loss of posture and generalized convulsion activity (Racine, 1972; Avignone et al., 2008). Mice progressed at least to stage 3 and were killed at 45 min and microglial morphology in the CA1 was analyzed. In some experiments AP5 (1.5 μg in 5 μl of ACSF) was applied 5 min before and 15 min after the intracerebroventricular application of KA.

Drugs. Glutamate, ATP, Brilliant Blue G (BBG), carbenoxolone (CBX), probenecid (PB), and NMDA were purchased from Sigma. CNQX, KA, TTX, and D-AP5 were purchased from Tocris Bioscience. Stock solutions of all drugs (except TTX) were made in water and diluted to the appropriate working concentrations in ACSF. The TTX stock was diluted in citric acid, pH 4.8. Sytox orange and propidium iodide were purchased from Invitrogen and used at a 1: 10,000 dilution. Drugs were applied to the slices either through bath application or through a PicoPump (WPI Pneumatic PicoPump). The diameter of the drug application pipette tip was ~3–4 μm. The pressure and duration of the puff can be controlled.

Uptake, extension, and process index analyses. For all index analyses, image analysis was done using ImageJ. Max projection images were collated to form time-lapse movies. Where necessary, movies were registered using the StackReg plugin to eliminate any *x-y* drift. For uptake index, an ROI was selected around each neuronal soma of interest. The florescence intensity of this ROI was determined using ImageJ and for statistical analysis, normalized data at 15 min following drug application were compared.

For extension index, ROIs in the cell body layer of the CA1 or cortex were cropped from movies to be analyzed. These regions were then binarized and an automated threshold was set on the ROI. The area of the suprathresholded regions of the projection stack was then measured through time and normalized to the area of the first frame of the movie to a starting index value of 1.0. The index through time of each time-lapse movie was then determined.

Process index analysis was done by two independent "blind" observers who manually counted the number of primary processes emanating from microglial somata in control mice and mice undergoing seizures. Data from the two observers were averaged. Microglial morphology analysis was performed on images using ImageJ. Images of individual microglia without overlapping territories with other microglia or blood vessels were selected for analysis. An automated threshold was set on each image and a particle analysis was performed on thresholded images. Microglial cell area was average and normalized to 100% for microglia from untreated mice and compared with microglia from mice that had undergone seizures.

Process velocity analysis. For process velocity analysis either directed toward an ATP-containing pipette or a laser-induced injury, time-lapse movies were first registered using the StackReg plugin to eliminate any *x-y* drift. Individual processes were then tracked using the Manual Tracking plugin. Migrating processes were selected at random but only processes that were maintained through at least five frames were used. The average process velocity through the tracked period was determined and averaged from five processes per experiment for three experiments.

Statistical analysis. For microglial extension analysis, four to six slices from different mice were analyzed and the data pooled to establish significance. For each figure, a different set of slices were analyzed. For electrophysiology, five cells were analyzed per condition. For *in vivo* analysis of wild-type mice undergoing seizures, 10 slices from control,11 slices from intraperitoneal KA-treated mice, 18 slices from intracerebroventricularly KA-treated mice, and 24 slices from mice receiving intracerebroventricular cotreatment with KA and AP5 (two to three mice

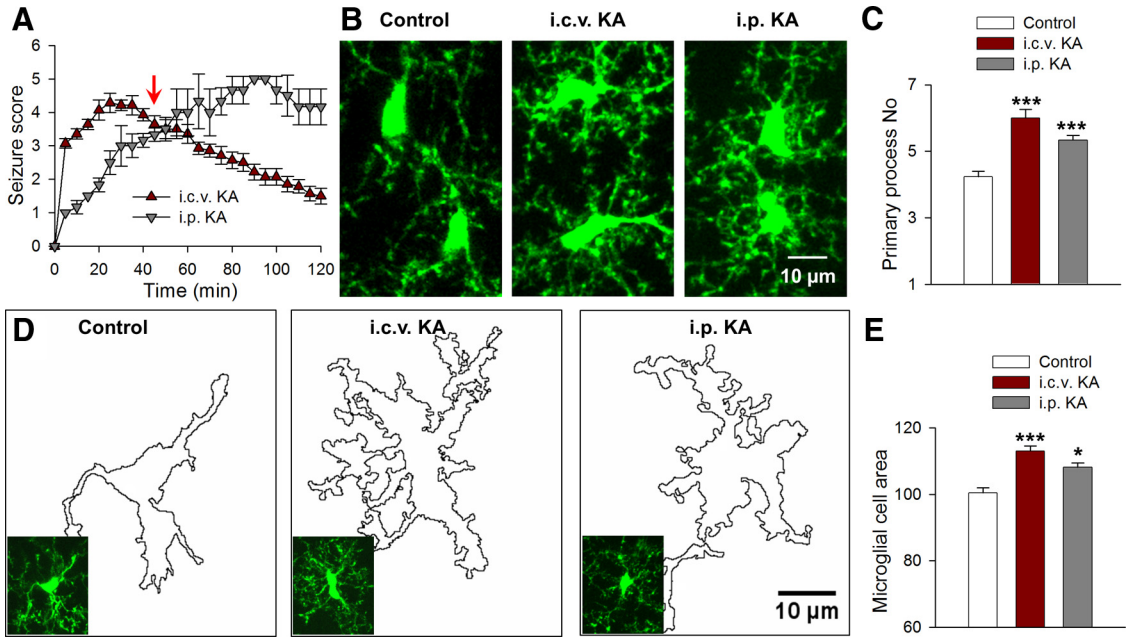

Figure 1. KA-induced seizures alter microglial morphology *in vivo*. ***A***, Seizure scores following intraperitoneal and intracerebroventricular injections of KA identifying the period in which microglial morphology was studied (red arrow). ***B***, Representative images of hippocampal microglia from control and KA-treated animals. ***C***, Quantitative data showing KA increases primary microglial branch numbers. ***D***, Outline of microglial morphologies in representative slices from control and KA-treated mice used to determine microglial area. ***E***, Quantitative normalized area showing KA increases microglial cell area; $*p < 0.05$, $***p < 0.001$.

each) were analyzed. For P2Y12 KO animals, analysis was performed on eight slices from three control and intracerebroventricularly KA-treated mice each. For all other experiments, the number of mice used is stated in the Results. Data are presented as mean ± SEM. Student's *t* test was used to establish significance.

Results

Acute seizure activity increases microglial process numbers

We induced status epilepticus in mice by both intraperitoneal (22 mg/kg) and intracerebroventricular (0.18 μg) injection of KA. Upon KA injection in both models, mice progressed to stage 3 of a modified Racine scale (see Materials and Methods) with continuous head bobbing signifying the onset of seizures ($n = 5$ mice each; Fig. 1*A*). To determine the effect of acute seizures on microglia, we killed mice 45 min after KA injection when seizures were significant and neuronal hyperactivities are well established in both models (Fig. 1*A*, red arrow). Microglial morphologies were then observed in fixed hippocampal slices. At this time point, microglia in the CA1 displayed a 25–40% increase in the number of primary processes (from 4.23 ± 0.17 to 5.33 ± 0.15 and 6.00 ± 0.26 processes following i.p. and i.c.v.) emanating from the microglial soma (Fig. 1*B*,*C*). Correspondingly, there was an 8–15% increase in the microglial cell area with the application of KA (Fig. 1*D*,*E*). Since epileptic seizures result in increased glutamate release (During and Spencer, 1993; Cavus et al., 2005; Meurs et al., 2008), these initial observations led us to investigate the effects of glutamate on microglial dynamics in acute hippocampal slices.

Glutamate induces microglial process extension in acute brain slices and *in vivo*

To test the possible regulation of microglial dynamics by neuronal activity, we applied glutamate to brain slices and monitored microglial responses by high-resolution two-photon microscopy in the CA1 region of the hippocampus. Under baseline conditions, microglial processes make random limited extensions and retractions in the neuropil. Glutamate (1 mM) elicited robust microglial process extension to the CA1 beginning at ~5 min of application ($n = 4$ slices, Fig. 2*A*,*E*). The effect was most pronounced in the stratum pyramidale (SP) with a high density of neuronal somata and less dramatic in the stratum radiatum (SR) or stratum oriens (SO).

Next, we asked whether this microglial response required neuronal firing induced by glutamate application. Interestingly, we found that microglial process extension in response to glutamate still occurred in the presence of TTX (extension index: 1.81 ± 0.2 without vs 1.94 ± 0.1 with TTX; $p > 0.05$), suggesting that the extension is independent of neuronal firing ($n = 5$ slices; Fig. 2*B*,*E*) even though electrophysiological recordings from neurons ($n = 5$) in the CA1 showed that glutamate induced action potential firing, which was inhibited by TTX (1 μM; Fig. 2*D*). Consistently, microglial process extension was not observed during neuronal depolarization by 10 mM K^+ (extension index: 0.96 ± 0.1 compared with control media change: 1.11 ± 0.1; $p > 0.05$; $n = 4$ slices; Fig. 2*C*,*E*). The glutamate-induced microglial process extension is concentration dependent as microglia lack responses at 0.1 mM ($n = 5$ of 5 slices tested slices) and responses occur in some slices at 0.5 mM glutamate ($n = 3$ of 10 slices tested; Fig. 2*F*).

To confirm that microglial responses are not due to neuronal cell death, we imaged slices incubated with Sytox, a membrane-impermeable DNA binding dye that labels nuclei of only dead/dying cells (Eyo and Dailey, 2012). We found that glutamate application did not induce Sytox uptake in neurons, though a laser-induced injury resulted in localized Sytox uptake within minutes (uptake index: 5.57 ± 2.1 during glutamate application vs 31.71 ± 4.0 after a laser burn injury; $n = 3$; $p < 0.001$; Fig. 2*G*). Similar results were obtained with propidium iodide (uptake index: 3.74 ± 7.9 during glutamate application vs 29.96 ± 11.6 after a laser burn injury; $n = 3$; $p < 0.01$).

To determine the ubiquity of this glutamate-induced microglial process extension, we examined microglial dynamics in

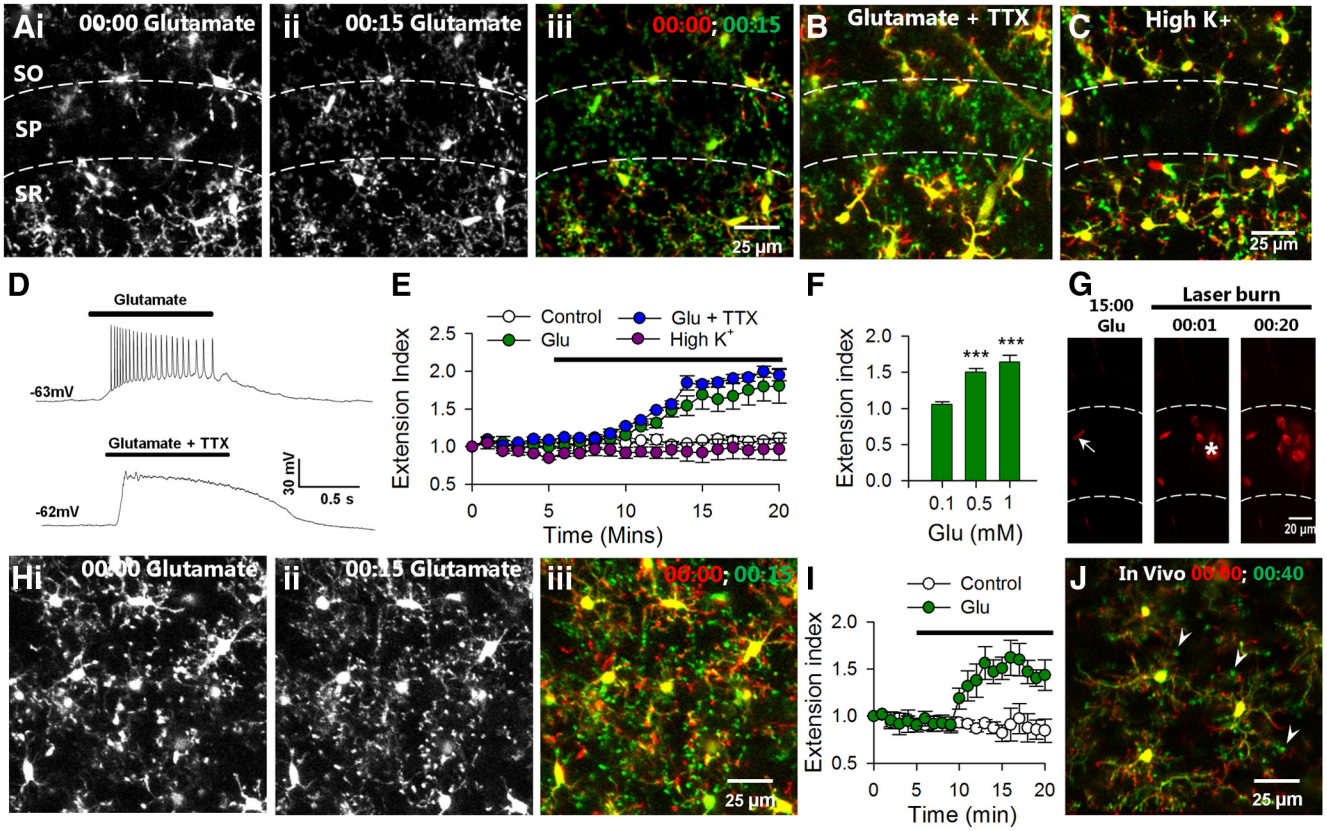

Figure 2. Glutamate induces microglial extension independent of action potential firing in slices and *in vivo*. ***A***, Representative two-photon images from time-lapse movies at the beginning (***i***) and 15 min (***ii***) of glutamate (1 mM) showing that glutamate induces microglial process extension in the CA1, which is merged (***iii***) as a color-coded image of microglial morphology at the beginning of glutamate application (red) and after 15 min of glutamate exposure (green). Extending processes are obvious (shown in green) following glutamate application. ***B***, Merged images from a time-lapse movie showing that TTX does not block glutamate-induced microglial process extension. ***C***, High K^+ does not induce microglial process extension. ***D***, Representative electrophysiological tracings showing that glutamate-induced action potentials are blocked by TTX (1 μM). ***E***, Quantitative summary of microglial process extension through time under control media change, high K^+, glutamate, and glutamate with TTX application from several experiments. ***F***, Average extension index at different concentrations of glutamate (note that $n =$ only 3 of 10 slices at 0.5 mM as there were no responses in the remaining 7 slices); $^{***}p < 0.001$. ***G***, Images from a time-lapse sequence of Sytox-labeled slices. Neurons are healthy and unlabeled during 15 min of glutamate (1 mM) application. The few labeled cells are crescent shaped like endothelial cells (arrow). Neurons take up Sytox after a laser burn-induced injury (asterisk). ***H–J***, Microglial processes extend during glutamate application in cortical slices (1 mM; ***H***, ***I***) as well as *in vivo* (5 mM; ***J***) with bulbous ending (***J***, arrowheads).

cortical slices. Indeed, we confirmed that glutamate elicited microglial process extension (extension index: 0.84 ± 0.1 in control vs 1.44 ± 0.2 with glutamate; $p < 0.001$) in cortical microglia, though to a lesser degree compared with hippocampal microglia ($n = 5$ slices; Fig. 2*H*,*I*). Finally, we performed *in vivo* two-photon imaging in the intact mouse brain and topically applied glutamate (5 mM) to an open cranial window. As in slices, we observed microglial process extension after several minutes of glutamate application *in vivo*. Moreover, extending microglia often had bulbous endings ($n = 3$ mice; Fig. 2*J*). Because we observed the most robust microglial response toward the CA1 region, we focused on this region for the rest of our studies.

Microglial processes make increasing contact with neuronal elements during glutamate exposure

The observation of microglial extension toward CA1 neuronal somata in slices and bulbous endings *in vivo* is reminiscent of direct microglia-to-neuron physical interactions (Wake et al., 2009; Li et al., 2012). Thus, our results suggest that microglia are attracted to contact neuronal elements during glutamate application. To provide direct evidence of microglial targeting to neuronal elements, we took advantage of Thy1-YFP transgenic mice that express YFP in a subset of pyramidal neurons in the hippocampus (Feng et al., 2000) and crossed them with the GFP-microglia line (Jung et al., 2000). In these double transgenic mice, we monitored microglial–neuronal interactions during glutamate application for 15 min each within the SP in acute slices. We imaged in CA1 regions with only a few labeled neurons that could easily be distinguished from microglia, which are much smaller with motile processes. We found that microglial processes interact with both neuronal dendrites (Fig. 3*A*) and neuronal somata (Fig. 3*B–E*) during glutamate application. Particularly, these processes made three times as many contacts with neuronal somata with characteristic bulbous endings during glutamate application ($n = 15$ neurons; Fig. 3*B–E*). These contacts were usually transient lasting for 1 min or 2 min. We did not observe dendritic beading of YFP neurons during glutamate exposure, again suggesting that neurons under our condition do not exhibit obvious morphological signs of damage.

Next, we wanted to determine a role for astrocytes in glutamate-induced microglial process extension. To this end, we used fluoroacetate (FAC), a known blocker of astrocytic function as shown in hippocampal slices (Pascual et al., 2012). We found that following a 60 min treatment of FAC (1 mM), microglia in slices still extended their processes toward the CA1 during a 15 min coincubation with glutamate (extension index: 1.95 ± 0.2 with and 2.01 ± 0.1 without FAC; $p > 0.05$; Fig. 3*F*,*G*). Our data

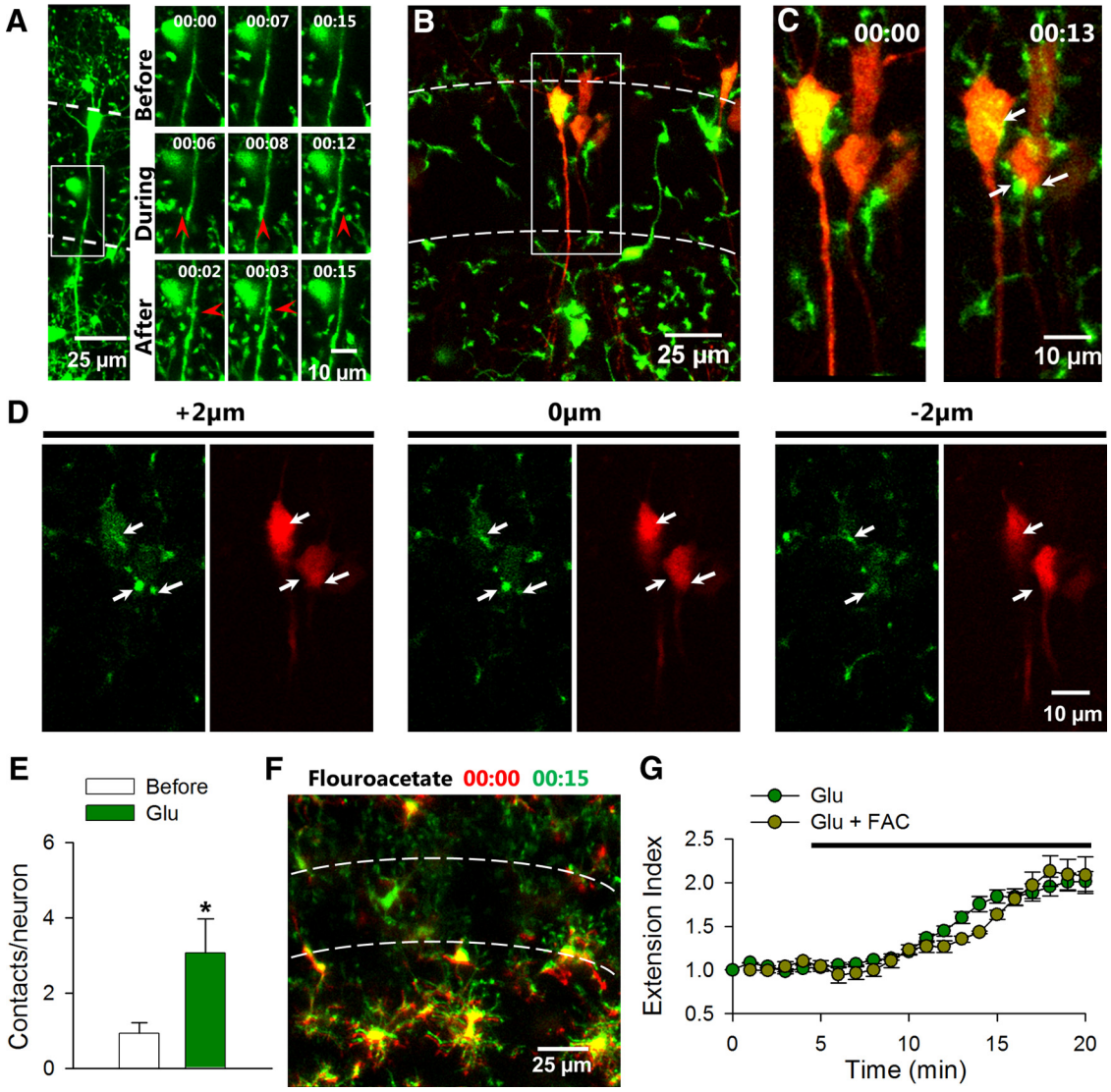

Figure 3. Glutamate increases microglial contact with neurons. ***A***, Left, Larger field of view showing neurons and microglia in CA1 in GFP-YFP double transgenic mice. Right, The boxed region in the left image shows that during and after glutamate application microglial processes make contact with neuronal dendrites in the SP. Points of contact are depicted with red arrowheads. ***B***, A *z*-stack projection of a representative hippocampal slice showing florescent microglia (green) and neurons (red) in GFP-YFP double transgenic mice. ***C***, Time-lapse images of the boxed region in ***B*** show microglial contact with neuronal somata. Points of contact are depicted with white arrows. ***D***, Single plane images of neurons and microglia in ***C*** at 2 μm intervals show contact (white arrows) in the same plane. ***E***, Quantitative data show that glutamate (1 mM) application increases microglial contact with neuronal somata. ***F***, Merge color-coded images from time-lapse movies of microglial process extension during glutamate application in the presence of astroglial toxin, FAC (1 mM). ***G***, Quantitative summary of microglial process extension during glutamate application with or without FAC (1 mM); $n = 15$ neurons in ***F*** and $^*p < 0.05$.

indicate that glutamate increases microglial contact of both neuronal somata and dendrites independent of astrocytic function.

Glutamate-induced microglial process extension requires NMDA receptors

We proceeded to determine the mechanism by which glutamate induces microglial process extension in the CA1 in hippocampal slices. First, glutamate receptor antagonists were applied to acute brain slices together with glutamate. We found that CNQX (10 μM), an AMPA and kainate receptor antagonist, failed to prevent the glutamate-induced microglial extension. However, AP5 (100 μM), a selective NMDA antagonist, completely abolished the glutamate-induced microglial process extension (extension index: 2.28 ± 0.2 with glutamate only, 2.07 ± 0.3 with glutamate and CNQX, and 1.06 ± 0.1 with glutamate and AP5; $p < 0.001$ with glutamate ± AP5 compared with glutamate only; $n = 5$ slices each; Fig. 4*A–D*). AP5 itself had no detectable effect on basal microglial properties including process extension in the SP (extension index: 0.96 ± 0.04 before and 1.01 ± 0.1 after AP5; $n = 3$; $p > 0.05$) or process dynamics in the SR (motility index: 41.26 ± 0.3 before, 41.11 ± 0.2 during, and 40.87 ± 0.1 after AP5 application; $n = 3$; $p > 0.05$). These results indicate that NMDA receptors but not AMPA/kainate receptors are necessary for glutamate-induced microglial responses.

Second, to further establish the glutamate receptor subtype(s) capable of eliciting microglial process extension, we applied selective glutamate receptor agonists. Application of KA (100 μM; $n = 5$ slices), which activates AMPA and kainate receptors, failed to induce microglial extension toward the SP. As with glutamate, application of NMDA (30 μM) elicited robust branch extension in the CA1, which was blocked by AP5 (extension index: 1.06 ± 0.1 with KA, 3.46 ± 0.1 with NMDA, and 1.01 ± 0.18 with

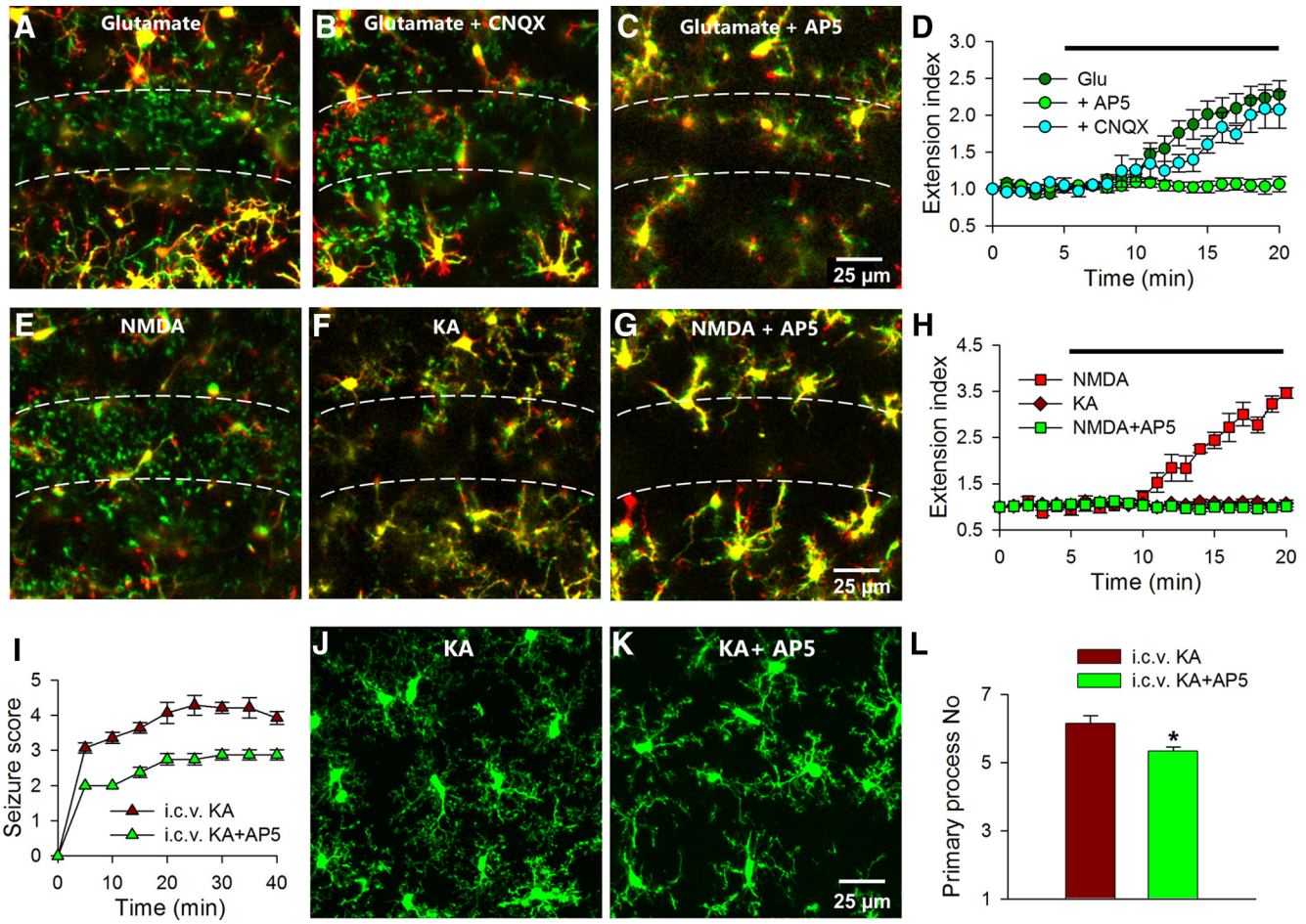

Figure 4. Glutamate induces microglial process extension through NMDA receptors. ***A–C***, Merged color-coded images from time-lapse movies showing that glutamate (1 mM) induces microglial extension (***A***) even in the presence of CNQX (10 μM; ***B***), but fails to do so in the presence of AP5 (***C***; 100 μM). ***D***, Quantitative summary of ***A–C***. ***E–G***, NMDA (30 μM) induces microglial process extension (***E***), which is blocked by AP5 (100 μM; ***G***), while KA (100 μM) fails to do so (***F***). ***H***, Quantitative summary of ***E–G***. ***I***, Seizure scores during intracerebroventricular delivery of KA in the presence or absence of AP5. ***J–L***, Qualitative images (***J***, ***K***) and quantitative summary (***L***) of microglial morphology at 45 min of intracerebroventricular KA delivery with or without AP5. AP5 reduces seizure-induced microglial morphological changes; $^*p < 0.05$.

NMDA and AP5; $p > 0.05$ with KA compared with control, $p < 0.001$ with NMDA compared with control, and $p < 0.001$ with NMDA ± AP5 compared with NMDA only; $n = 4–5$ slices each; Fig. 4*E–H*). These results suggest that activation of the NMDA receptor is sufficient for inducing microglial process extension.

Given these observations in slices, we returned to the acute intracerebroventricular KA-induced seizure model to determine the role of NMDA receptors in seizure-induced microglial morphological alterations. We were able to detect a significant reduction in seizure phenotypes after intracerebroventricular application of AP5 (1.5 μg) together with KA (0.18 μg; Fig. 4*I*). Additionally, AP5 reduced the primary process numbers of hippocampal microglia after seizure in fixed slices (Fig. 4*J–L*). Therefore, these results indicate that seizure-induced changes in microglial processes require NMDA receptor activation reminiscent of the phenomena in slices.

Activation of neuronal NMDA receptors recruits microglial processes through purinergic signaling

Microglia have been suggested to express functional NMDA receptors (Kaindl et al., 2012). However, we found that in hippocampal slices, although neurons responded robustly to localized puffs of glutamate, microglia lacked electrical responses to localized puffs of either glutamate or NMDA ($n = 5$ cells; Fig. 5*A*). Therefore, the glutamate-induced microglial process extension is most likely mediated by neuronal but not microglial NMDA receptors. Consistent with our electrophysiological results, we also confirmed that NMDA does not serve as a direct chemoattractant to microglia. Localized puffs of NMDA (100 μM at 5 psi for 10 s) through a pipette failed to induce microglial process extension (Fig. 5*B*). However, replacement of the pipette with ATP (3 mM at 5 psi for 1 s) resulted in robust microglial process extension toward the pipette tip at the same loci (2.67 ± 1 extending processes during NMDA application vs 64.33 ± 5 extending processes during ATP application; $n = 3$ experiments; $p < 0.001$; Fig. 5*B*). These results suggest that purinergic signaling could be the secondary signal(s) responsible for microglial process extension during NMDA receptor activation.

To test the idea that purinergic signaling mediates NMDA receptor-dependent microglial process extension, we first abolished endogenous ATP gradients by incubating brain slices with ATP (1 mM). Indeed, in the presence of ATP, NMDA-induced microglial extension toward the CA1 was significantly reduced (extension index: 2.71 ± 0.3 in NMDA only vs 1.04 ± 0.1 with NMDA and ATP; $n = 6$ slices; $p < 0.001$; Fig. 5*C*,*E*). The P2Y12 receptor is known to mediate ATP-induced microglial process chemotaxis (Haynes et al., 2006; Wu et al., 2007). Therefore, P2Y12 KO mice were used to directly test the role of purinergic

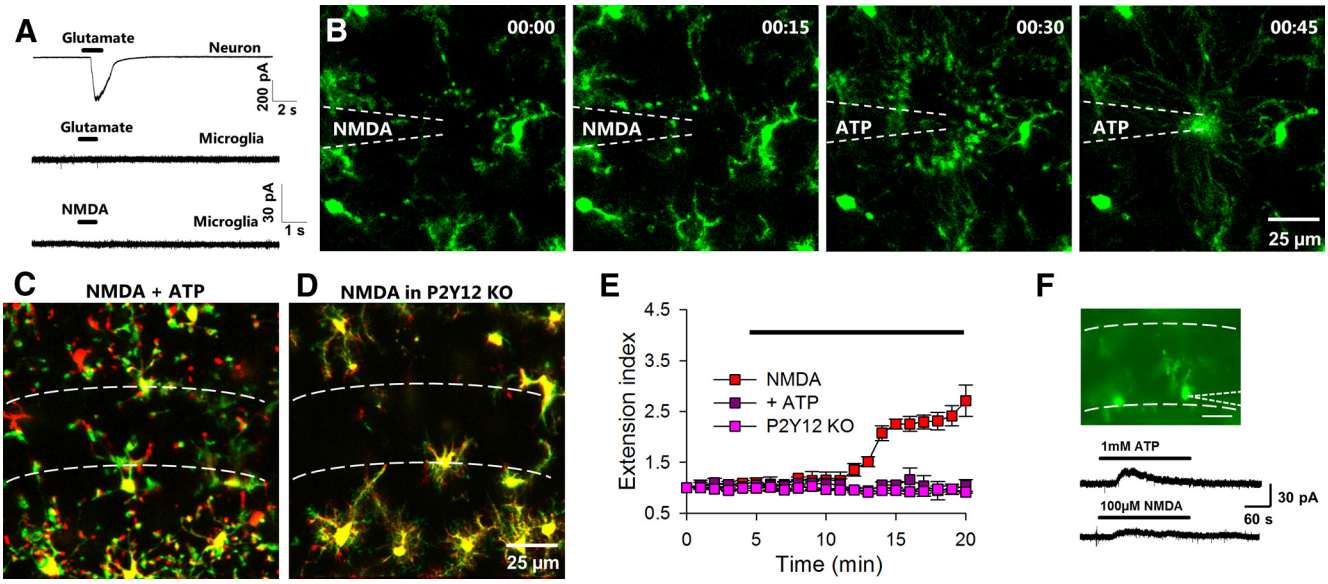

Figure 5. NMDA-induced microglial process extension requires purinergic signaling and P2Y12 receptor. ***A***, CA1 neurons show large inward currents to puff application of glutamate (top trace) while microglia show no current responses to either glutamate (middle trace) or NMDA (bottom trace). ***B***, Puff application of NMDA (100 μM; 5 psi for 10 s) fails to induce microglial process extension while puff application of ATP (3 mM; 5 psi for 1 s) induces microglial process extension directly toward the pipette tip. ***C***, ***D***, NMDA (30 μM) fails to induce robust microglial process extension in the presence of ATP (1 mM; ***C***) or in P2Y12 KO tissues (***D***). ***E***, Quantitative summary of the data presented in ***C*** and ***D***. ***F***, Top, Epifluorescence image of patched microglia in the CA1. Bottom, Representative tracing showing that bath application of ATP- and NMDA-induced outward currents in patched microglia in the CA1.

signaling in glutamate-induced microglial process extension. Consistently, we found that NMDA failed to induce microglial process extension in slices from P2Y12 KO mice (extension index: 0.91 ± 0.02; $n = 4$ slices; $p < 0.001$ compared with NMDA only; Fig. 5*D*,*E*). These results suggest that ATP is the chemoattractant that activates microglial P2Y12 receptors to mediate glutamate-induced process extension.

To further confirm that purinergic signaling is secondary to neuronal activation of NMDA in glutamate-induced microglial process extension, we took an electrophysiological approach to record microglial ATP responses. We predicted that if microglia are responding to endogenously released ATP upon NMDA application, then microglia in close proximity to the SP will display ATP-induced outward potassium currents, as we have reported previously (Wu et al., 2007; Wu and Zhuo, 2008). Therefore, microglia in the CA1 layer were recorded using the whole-cell patch-clamp technique (Fig. 5*F*, top). Indeed, following NMDA bath application (100 μM; $n = 5$ of 8 cells), we detected outward currents similar to the ATP-induced current in microglia proximal to the SP (Fig. 5*F*). Similar results were observed with bath application of glutamate (1 mM; data not shown). However, as we have shown, direct puff application of NMDA to microglia was not able to induce the detectable current (Fig. 5*A*). These results suggest that the activation of neuronal NMDA receptors trigger ATP-dependent microglia process extension and outward currents.

Calcium- and channel-dependent ATP release inducing microglial process extension

We wanted to understand the potential mechanisms for ATP release that induce microglial process extension after neuronal NMDA receptor activation. Since the NMDA receptor is highly calcium permeable, we predicted that calcium influx via NMDA receptors triggers ATP release. To test this hypothesis, we first confirmed that NMDA application induces a significant increase in cytosolic calcium levels in CA1 neurons that are loaded with Ca^{2+} indicator, OGB in hippocampal slices (Fig. 6*A*–*C*). The NMDA-induced cytosolic calcium rise was largely reduced in the presence of TTX (1 μM) in nominally free calcium media (Fig. 6*A*–*C*). We further found that in nominally free calcium media, neither NMDA (extension index: 2.71 ± 0.3 in NMDA vs 1.03 ± 0.1 in calcium-free NMDA; $p > 0.001$; $n = 4$ slices; Fig. 6*D*,*F*) nor glutamate (data not shown) could induce microglial process extension. The removal of extracellular calcium itself did not limit microglial motility, as microglial process chemotaxis to an ATP-containing pipette under nominally free calcium conditions had similar velocities to that under control conditions (1.3 ± 0.07 μm/min in control and 1.2 ± 0.09 μm/ min; $p > 0.05$; Fig. 6*E*,*G*). These results suggest that Ca^{2+} influx is required for NMDA receptor-induced ATP release and microglial process extension.

Ion channels, such as the P2X7 receptor, connexin, and pannexin channels have been shown to be important avenues for ATP release (Kang et al., 2008; MacVicar and Thompson, 2010). Therefore, we tested the ability of BBG (a P2X7 antagonist), CBX (a connexin channel blocker), and PB (a pannexin channel blocker) to inhibit microglial process extension to NMDA. While BBG (10 μM; extension index: 2.71 ± 0.2; $n = 4$ slices) and CBX (50 μM; extension index: 2.68 ± 0.3; $n = 4$ slices) failed to block NMDA-induced microglial process extension, PB at a relatively high concentration (5 mM) effectively abolished the microglial process response to NMDA (extension index: 1.0 ± 0.02; $p < 0.001$; $n = 5$ slices; Fig. 6*H*–*K*). These results suggest that calcium influx through NMDA receptors is required for ATP release possibly through pannexin channels which elicit microglial process extension.

Glutamate-induced microglial process extension is not due to acute neuronal injury

A recent study in the intact zebrafish optic tectum suggested that laser-induced injury results in microglial attraction in an NMDA receptor-dependent manner (Sieger et al., 2012) leaving open the possibility that glutamate-induced microglial process extension in our system results from acute neuronal injury. Moreover, NMDA

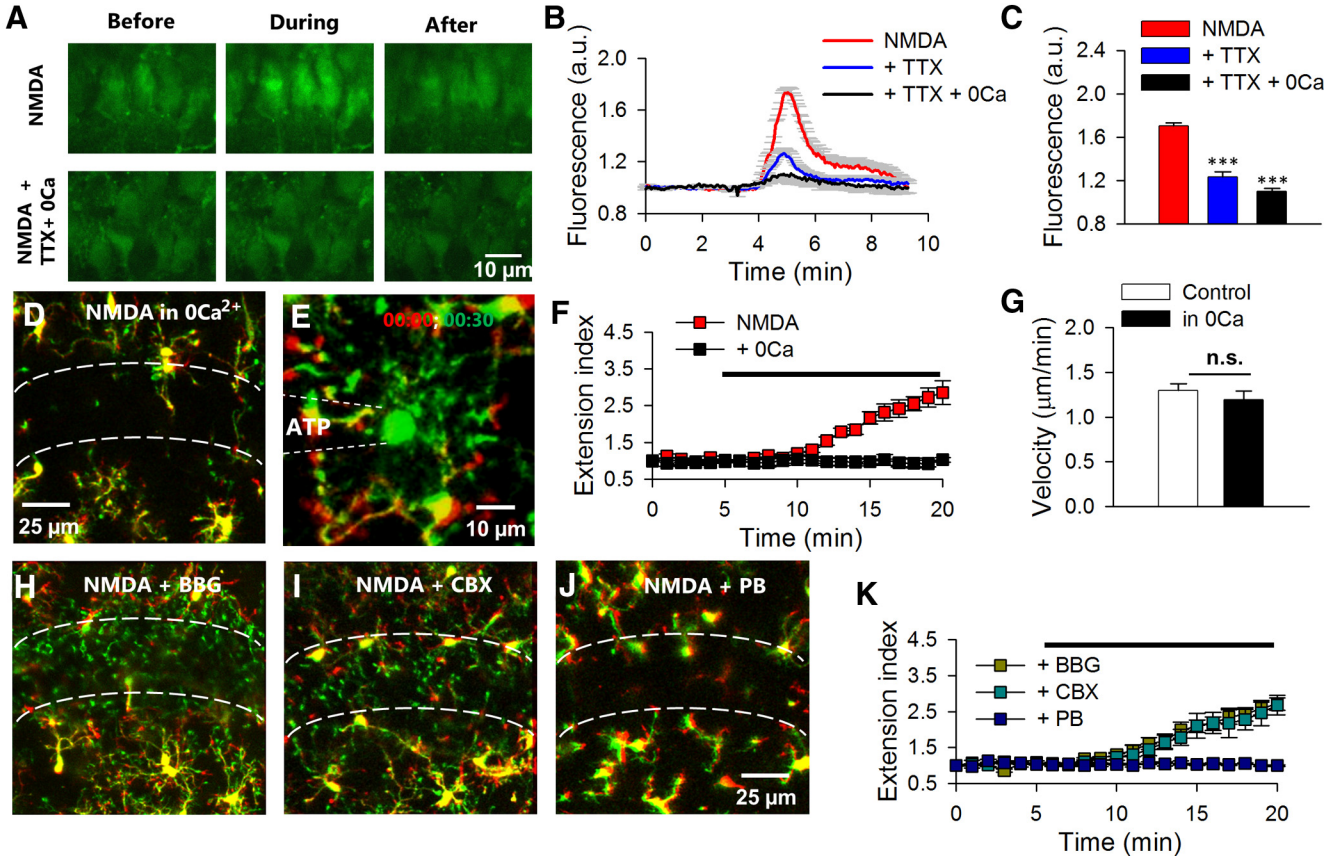

Figure 6. NMDA-induced microglial process extension requires calcium influx and purine release from pannexin channels. ***A–C***, Qualitative images of OGB-loaded hippocampal CA1 neurons before, during, and following a 2 min application of NMDA in normal ACSF (***A***, top) and in TTX containing nominally free calcium ACSF (***A***, bottom) with the quantitative summary in ***B*** and ***C***. ***D***, ***F***, Representative image (***D***) and quantitative summary (***F***) showing that in the absence of extracellular calcium, microglial process extension to NMDA is abolished. ***E***, Sample color-coded image of an ATP-induced chemotaxis at the beginning (00:00; red) and 30 min (00:30; green). Dashed lines indicate the location of the pipette. ***G***, Quantitative data show similar extension velocities with or without extracellular calcium during ATP application through a pipette. ***H–J***, Microglial process extension still occurs in the presence of P2X7 receptor antagonist BBG (10 μM; ***H***) and connexin channel blocker CBX (50 μM; ***I***) but not in the presence of pannexin channel blocker PB (5 mM; ***J***). ***K***, Quantitative summary of process extension under various conditions in ***H–J***; ***$p < 0.001$. a.u., arbitrary units.

induced delayed neurotoxicity evidence by propidium iodide uptake (albeit after prolonged periods of exposure) in organotypic hippocampal slices (Vinet et al., 2012). To rule out neurotoxic mechanisms, we incubated slices with propidium iodide, which labels dead/dying cells in the presence of glutamate or NMDA followed by a laser-induced injury to serve as a positive control. During NMDA (and glutamate) application, microglial processes extended but neurons did not take up the dye until there was a laser-induced injury after 15 min of glutamate/NMDA exposure wherein several cells around the lesion took up the dye (Figs. 2*G*; 7*A–C*). These results suggest that glutamate-induced/NMDA-induced microglial responses occur independent of overt neuronal injury.

Next, we performed laser injury-induced experiments and monitored microglial process extension to the site of injury. Microglial processes encircled the spherical laser-injury site within 30 min (Fig. 7*D*). Microglia still responded robustly to laser-induced injury under nominally free calcium conditions (Fig. 7*E*) and in the presence of 100 μM AP5 (Fig. 7*F*). However, microglial response to laser-induced injury was drastically reduced at 30 min in P2Y12 KO mice (Fig. 7*G*). Therefore, our results indicate that acute neuronal injury-induced microglial response is NMDA receptor independent but P2Y12 receptor dependent in the mouse hippocampus.

To further test the idea, we developed a protocol to selectively injure single neurons in the CA1 and monitored microglial responses (see Materials and Methods). We performed imaging in slices with YFP-labeled neurons and monitored Sytox uptake concurrently to confirm that our protocol only injured one neuron. Single neuron ablation resulted in an immediate loss of YFP in the selected neuron among many YFP-labeled neurons in the CA1 (Fig. 7*H,I*). Moreover, the nucleus of only this neuron took up Sytox indicating the selectivity of our protocol (Fig. 7*J*). As expected, in response to a localized laser-induced injury of a single neuron in the CA1, microglial processes extended toward the injury site within minutes (Fig. 7*K*). Consistently, blockade of NMDA receptor activation with AP5 (100 μM; Fig. 7*H*) or calcium removal during neuronal ablation did not prevent microglial process extension to the injury site (process extension velocity 2.92 $\pm$ 0.2, 2.59 $\pm$ 0.1, and 2.90 $\pm$ 0.1 μm/min under control, calcium removal, and AP5-treated conditions; $n = 15$ total processes analyzed from three experiments in each condition; $p > 0.05$). These results suggest that glutamate-induced microglial process extension toward hippocampal neurons occurs independent of acute neuronal injury.

P2Y12 receptor deficiency worsens acute experimental seizures

Given that the P2Y12 receptor is required for microglial process extension during neuronal hyperactivities, we attempted to determine the functional significance of these observations using P2Y12-deficient mice. We induced experimental seizures by KA injection *in vivo* in age-matched wild-type and P2Y12 KO ani-

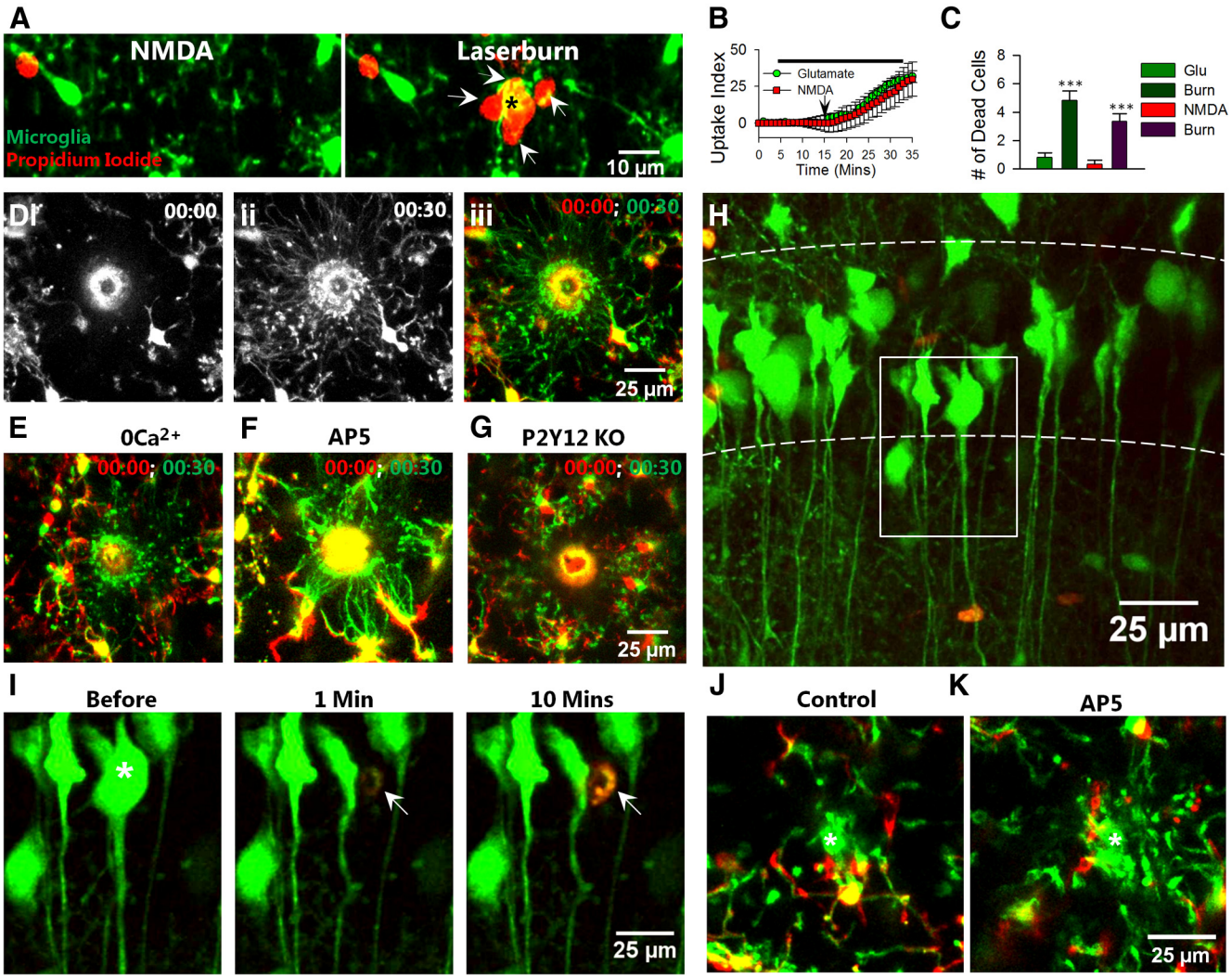

Figure 7. Injury-induced microglial process extension does not require NMDA receptors or calcium influx. ***A***, Time-lapse images of microglia (green) during NMDA application (left) and following a laser-induced injury (asterisk, right) in the presence of propidium iodide (red). ***B***, Propidium iodide uptake following laser-induced injury but not following glutamate/NMDA application. Arrow indicates time point of laser-induced injury. ***C***, Number of propidium iodide-positive cells after application of glutamate, NMDA, and a corresponding laser burn. ***D***, Laser-induced tissue injury induces robust microglial extension toward the injury site in control slices. ***E–G***, Microglial processes still extend toward the injury site in the absence of extracellular calcium (***E***, $0Ca^{2+}$) and presence of AP5 (***F***, 100 μM) but not in P2Y12 KO slices (***D***). ***H***, YFP-labeled neurons (green) in the presence of Sytox (red) in the CA1 of the hippocampus. ***I***, Neurons in the boxed region in ***H*** before, 1 min, and 10 min after single-cell ablation. The neuron to be ablated is identified with a white asterisk. Subsequent to laser ablation, Sytox (red; white arrow) is taken up by the single neuron. ***J***, ***K***, Representative merged color-coded images of microglial processes before (red) and 15 min after (green) single neuron ablation under control (***J***) and in the presence of AP5 (100 μM; ***K***). The ablation site is identified with a white asterisk; ***$p < 0.001$.

mals. Intraperitoneal delivery of KA (18 mg/kg) in P2Y12 KO mice resulted in worsened seizures (Fig. 8*A*). By 2 h of seizure observations, wild-type mice displayed an average seizure score of 2.0 ± 0.5 ($n = 11$) while P2Y12 KO mice displayed an average seizure score of 4.71 ± 0.9 ($n = 7$; $p < 0.05$). In addition, P2Y12 KO mice exhibited a significantly earlier onset of stage 3 seizures at 27.0 ± 1.8 ($n = 5$ of 7 animals) compared with 43.3 ± 3.0 min in wild-type mice ($n = 9$ of 11 animals; $p < 0.01$; Fig. 8*B*). Finally, although none of the 11 wild-type mice died during testing, three of the seven (i.e., 43% of) P2Y12 KO mice died during the 2 h observation period (Fig. 8*C*).

Previous studies have shown that P2Y12 receptors are exclusively expressed in microglia in the CNS (Sasaki et al., 2003; Haynes et al., 2006; Kobayashi et al., 2008; Tozaki-Saitoh et al., 2008; Butovsky et al., 2014). However, P2Y12 receptors are also present on peripheral platelets, which may complicate our above results with an intraperitoneal KA delivery route. To confirm that central (microglial) P2Y12 receptor function can modulate acute seizure phenotypes, we repeated seizure experiments by an intracerebroventricular KA delivery route. Remarkably, seizure phenotypes in P2Y12 KO mice were significantly increased compared with age-matched wild-type mice with a delivery of intracerebroventricular KA (0.12 μg; Fig. 8*D*). After 2 h of KA injection, wild-type mice exhibited an average seizure score of 1.25 ± 0.2 ($n = 8$) while P2Y12 KO mice displayed an average seizure score of 3.5 ± 0.8 ($n = 6$; $p < 0.05$). Furthermore, P2Y12 KO mice experienced a significant number of seizure spells characterized by brief period of intense seizures (range 8–23) compared with wild-type mice (range 0–4) during the 2 h observation period (1.5 ± 0.5 in wild-type, $n = 8$; 12.75 ± 2.5 in P2Y12 KOs, $n = 6$; $p < 0.01$). Moreover, only 50% of wild-type mice progressed to stage 4 seizures at this drug concentration while all P2Y12 KO mice experienced stage 4 seizures.

Consistent with our experiments in slices, although hippocampal microglial process numbers were similar between P2Y12 wild-type and KO microglia without seizures (4.23 ± 0.17

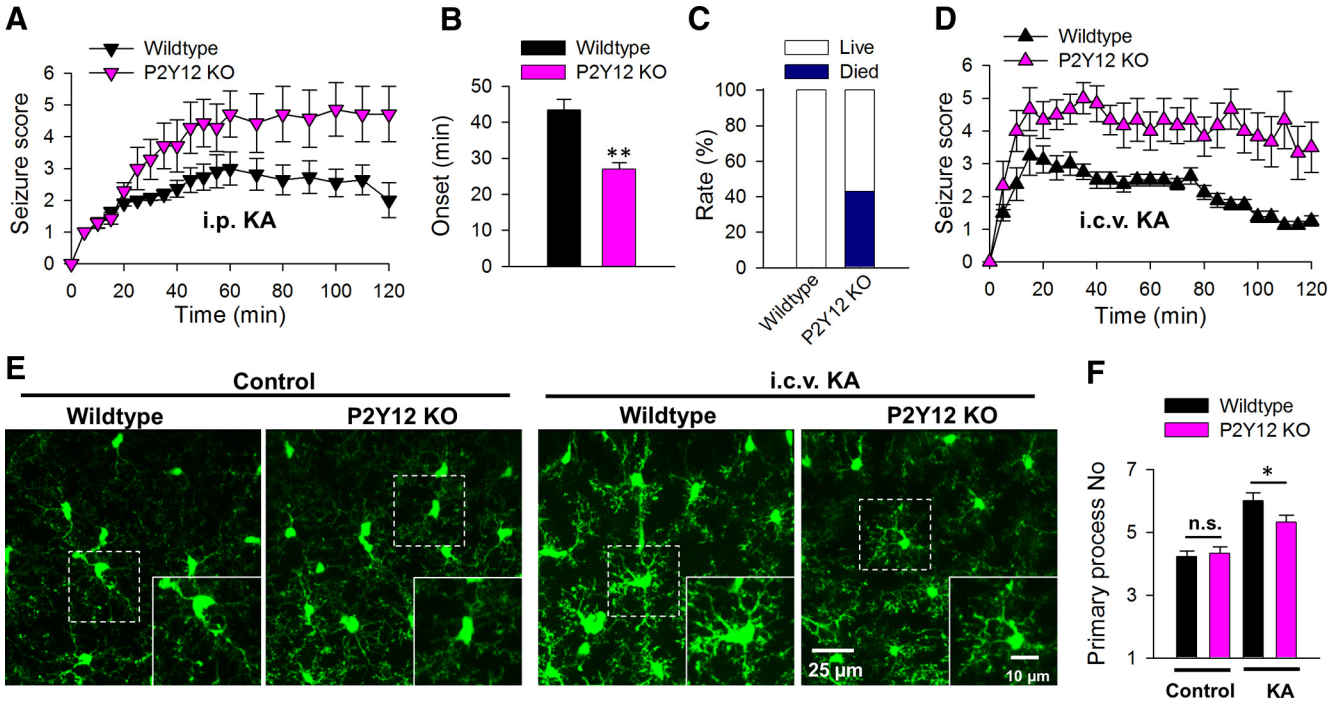

Figure 8. P2Y12 KO mice exhibit exacerbated seizure phenotypes and reduced microglial process numbers. ***A***, Acute seizure scores in wild-type and P2Y12 KO mice following intraperitoneal injection of KA. ***B***, Timing to seizure onset (stage 3 on the Racine scale) in wild-type and P2Y12 KO mice following intraperitoneal KA injection. ***C***, Animal survival/ mortality rates in wild-type and P2Y12 KO mice following intraperitoneal KA injection. ***D***, Acute seizure scores in wild-type and P2Y12 KO mice following intracerebroventricular injection of KA. ***E***, ***F***, Representative images of hippocampal microglia in the CA1 from wild-type and P2Y12 KO tissues under control and 45 min after intracerebroventricular KA conditions (***E***) and the corresponding quantitative data of microglial primary process numbers (***F***); $*p < 0.05$, $**p < 0.01$.

and 4.33 ± 0.21; $p > 0.05$), P2Y12 KO mice exhibited a significantly less dramatic increase in hippocampal microglial process numbers in fixed slices 45 min after drug delivery (6.00 ± 0.26 in wild-type vs 5.33 ± 0.22 in P2Y12 KO animals; $p < 0.05$; Fig. 8*F*). Finally, while wild-type mice generally recovered well by 2 h of the KA drug delivery, 50% of P2Y12 KO mice continued to experience seizures for several hours after the 2 h time point (data not shown). These results indicate that a genetic deficiency in P2Y12 receptors exacerbates acute seizures, suggesting neuroprotective roles for P2Y12-dependent microglia responses.

Discussion

Our current findings indicate that elevated glutamate levels activate neuronal NMDA receptors leading to calcium influx and ATP release, which elicit microglial process attraction through P2Y12 receptors (Fig. 9). Therefore, microglia employ P2Y12 receptors to interact with neurons during periods of increased glutamatergic signaling such as during epilepsy in the mammalian brain. Functionally, a lack of microglial P2Y12 receptors exacerbated seizure outcome associated with reduced microglia primary process numbers, suggesting that microglial process extension during glutamate treatment and experimental seizures serve a neuroprotective function. This is the first description of such neuron-to-microglia communication axis using a combinatorial approach including high-resolution live cell imaging, electrophysiology, and behavioral analysis.

Neuronal control of microglial dynamics in the mammalian CNS

Recent studies in the developing zebrafish indicated that microglial responses to laser-induced injury are mediated by calcium signaling acting through NMDA receptors (Sieger et al., 2012) and that uncaged glutamate, acting on neurons, can steer microglial processes toward the site of glutamate release (Li et al., 2012). Our results now provide direct evidence for neuronal influence on microglial dynamics in the mammalian brain. In particular, we show dramatic differences between the mammalian and zebrafish systems in terms of injury-induced microglial responses. In the zebrafish, both calcium influx and NMDA receptors were required for microglial migration to the site of a neuronal laser injury (Sieger et al., 2012). However, in the mouse, neuronal injury induced by a laser did not require NMDA receptors or calcium influx, suggesting that microglial responses are regulated by differing mechanisms in these species.

Previous work in mammalian tissues on glutamate-induced microglial responses had focused on the spinal cord (Liu et al., 2009) and retina (Fontainhas et al., 2011). The former study reported that glutamate induces microglial migration in culture and in spinal cord slices through AMPA and metabotropic glutamate receptors independent of purinergic signaling (Liu et al., 2009). The latter study failed to elicit significant morphological changes in retinal microglia upon either glutamate or NMDA application (Fontainhas et al., 2011). Unlike that in culture and spinal cord slices, we never observed microglial migration in response to glutamate or NMDA within 1–2 h of the generation of hippocampal or cortical slices. Moreover, microglial responses to glutamate in brain slices require neuronal NMDA receptors and purinergic signaling. Interestingly, while Fontainhas et al. (2011) reported increased microglial dynamism to kainate and AMPA glutamate receptor agonists in retinal explants, our results show that KA, which activates both kainate and AMPA recep-

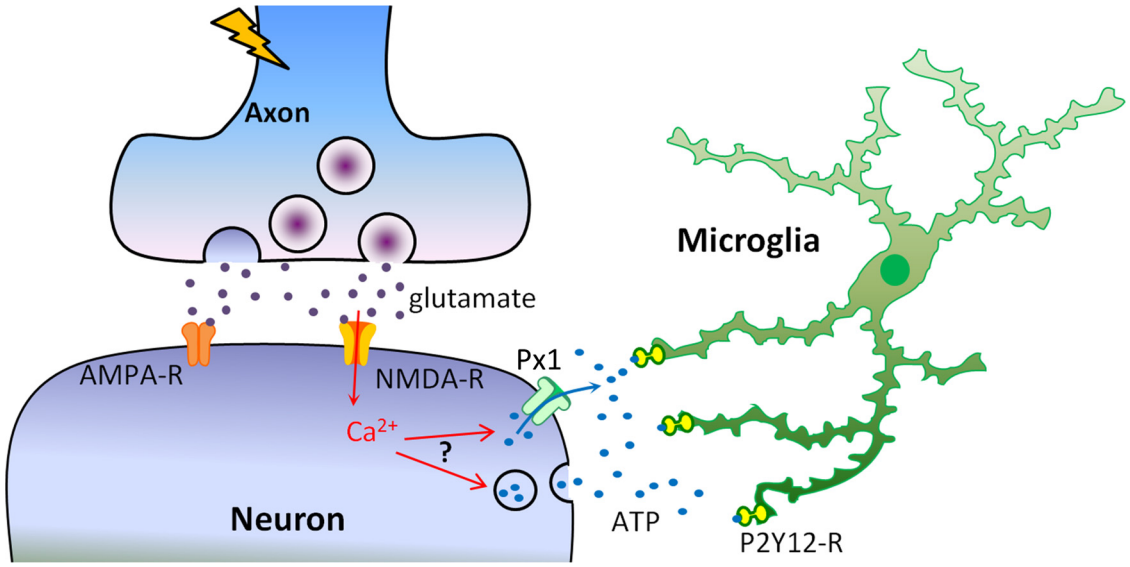

Figure 9. Schematic model for glutamate-induced microglial process extension in epilepsy. During periods of intense neuronal hyperactivity as occurs in epilepsy, neurons release glutamate from presynaptic terminals that can activate AMPA receptors (AMPA-R) and NMDA receptors (NMDA-R) on postsynaptic sites. The NMDA-R activation leads to influx of extracellular calcium and such elevations of cytosolic calcium, through currently unknown mechanisms, result in the release of ATP possibly through either ion channels like pannexin 1(Px1) or prepackaged vesicles. Released ATP diffuses into the extracellular space forming a chemotactic gradient that activates microglial P2Y12 receptors (P2Y12-R) to induce microglial process extension toward neuronal elements.

tors, failed to elicit microglial branch extension in acute brain slices. Activation of glutamatergic signaling may have similar effects on retinal and cerebral microglia but may differ in the spinal cord.

Molecular mechanisms underlying glutamate-induced microglial process extension

Although microglial–neuronal interactions *in vivo* are modulated by neuronal activity (Wake et al., 2009; Tremblay et al., 2010), precise mechanisms involved have not been addressed. It has been suggested that microglia express NMDA receptors (Murugan et al., 2011; Kaindl et al., 2012). In our study, we did not detect electrophysiological or morphological responses to NMDA in microglia suggesting that resting microglia in the hippocampus lack functional NMDA receptors. Consistently, glutamate could not induce any detectable current in brain microglia (Wu and Zhuo, 2008; Fontainhas et al., 2011). However, we cannot rule out the possibility of the existence of functional NMDA receptors on a very small subset of resting microglia in the brain. Interestingly, here we found that NMDA-dependent microglial responses occur independent of neuronal action potentials, which is consistent with previous work in the mouse cortex *in vivo* showing that basal microglial sampling occurs independent of action potentials (Nimmerjahn et al., 2005). Our calcium-imaging data also indicate that this occurs despite the fact that TTX dramatically reduces the NMDA-induced intracellular calcium elevations. These results argue that the microglial response is more highly sensitive to NMDA-induced calcium rises than by action potentials.

Microglial chemotaxis has been suggested for several chemoattractants including purines (ATP/ADP), fractalkine, nitric oxide, and fibrinogen (Davalos et al., 2005; Wu et al., 2007; Liang et al., 2009; Dibaj et al., 2010; Davalos et al., 2012). Although we have not ruled out the involvement of other chemoattractants, the lack of a microglial response in P2Y12 KOs to NMDA suggest the exclusive involvement of purinergic signaling. Microglial chemotaxis to sources of ATP have been extensively studied and shown to require both purinergic P2 receptors (Haynes et al., 2006; Wu et al., 2007) and P1 adenosine receptors (Färber et al., 2008; Ohsawa et al., 2012). Moreover, both chloride and potassium channels (Wu et al., 2007; Hines et al., 2009) are required in the process. Thus, adenosine receptors along with potassium and chloride channels are sure to participate in microglia process extension toward hyperactive neurons as well.

We found that PB, a widely used pannexin blocker, was able to abolish glutamate-induced microglial process extension. Several studies have shown that pannexin opening can occur as a result of increases in intracellular calcium concentrations leading to subsequent ATP release (Locovei et al., 2006; Huang et al., 2007; Kurtenbach et al., 2013; Orellana et al., 2013). Consistent with this, we found that microglial responses during NMDA/glutamate application were abolished in nominally free calcium-containing media suggesting that NMDA receptor activation induces elevations in cytosolic calcium levels before ATP release. However, a previously reported NMDA–pannexin coupling in hippocampal slices did not require calcium influx (Thompson et al., 2008). Moreover, although in our studies PB could inhibit NMDA-induced microglia process extension, a relatively high concentration was needed. Therefore, our results suggest that non-pannexin mechanisms, such as vesicle-dependent ATP release, may be involved. Further work with pannexin KO mice will be required to ascertain the role of pannexin channels in glutamate-induced microglial process extension. Nevertheless, our results suggest that the avenue of ATP release is PB sensitive even if not pannexin dependent.

Microglia–neuron communication in epilepsy

Epilepsy poses a significant social concern as it is the third most common brain disorder and current therapeutic strategies have proven insufficient in at least one-third of patients (Vezzani et al., 2011). Microglia remain controversial cells of the CNS with both beneficial and detrimental roles attributed to them especially within the context of disease pathology (Wu et al., 2012; Eyo and Dailey, 2013). Our results *in vivo* indicate for the first time that acute seizure activity modulates microglial morphology in an NMDA-dependent manner, which is consistent with the data in

slices. However, KA application elicited changes in microglial morphology *in vivo* but it failed to alter microglial process dynamics in slices. Our data suggest that KA induces glutamate release that could activate NMDA receptors *in vivo*. Therefore, the lack of microglial responses to KA in slices may indicate that (1) sufficient glutamate is not released to elicit the microglial effect in slices and/or (2) glutamate accumulation persists *in vivo* as a result, for example, of a seizure-induced failure of glutamate uptake mechanisms (Ueda et al., 2001) that may not occur in slices. Nevertheless, we acknowledge that by the nature of the case, slice experiments are not entirely representative of the *in vivo* condition.

We found that microglial responses were more robust in the hippocampus than in the cortex. The reason for this is not clear, but at least two attractive possibilities exist: (1) a higher density of neurons in hippocampal CA1 relative to the cortical layers II/III or (2) differences in neuronal subtypes in these brain regions. In addition, whether microglial process extensions in response to glutamate occur during physiological conditions are unclear. Our results suggest that they are most relevant to conditions with increased glutamatergic signaling because microglial responses in slices required 0.5 mM or higher of glutamate, which is well beyond normal physiological levels. Finally, the acute nature of the microglial responses in slices (5–8 min of glutamate/NMDA exposure) and seizures (within 45 min of KA delivery) suggest that these responses precede neuronal death, which requires prolonged (up to 4 h) excitotoxic challenge in organotypic hippocampal slices (Vinet et al., 2012) or during seizures (24–48 h) *in vivo* (Avignone et al., 2008).

What is the functional consequence of microglial contact of neuronal elements during glutamatergic signaling? A recent study in the zebrafish suggested that microglial contact of neuronal somata serves to downregulate neuronal hyperactivity (Li et al., 2012). Another interesting observation is that, during tissue injury, microglial process chemotaxis has been shown to play neuroprotective roles in curtailing the expansion of the injury site in the mammalian brain (Hines et al., 2009). Consistent with this, we present compelling data that microglial P2Y12 receptors serve neuroprotective functions during acute seizures. Considering the impaired microglial process extension to neuronal hyperactivities, these results suggest the potential neuroprotective function of microglial process extension in epilepsy. Future studies are needed to understand the molecular mechanisms underlying the neuroprotective function of microglial contact of neurons. When determined, it could serve as a novel therapeutic strategy against neuronal hyperactivity in such chronic disorders as epileptic seizures.

References

Avignone E, Ulmann L, Levavasseur F, Rassendren F, Audinat E (2008) Status epilepticus induces a particular microglial activation state characterized by enhanced purinergic signaling. J Neurosci 28:9133–9144. CrossRef Medline

Beach TG, Woodhurst WB, MacDonald DB, Jones MW (1995) Reactive microglia in hippocampal sclerosis associated with human temporal lobe epilepsy. Neurosci Lett 191:27–30. CrossRef Medline

Boucsein C, Kettenmann H, Nolte C (2000) Electrophysiological properties of microglial cells in normal and pathologic rat brain slices. Eur J Neurosci 12:2049–2058. CrossRef Medline

Butovsky O, Jedrychowski MP, Moore CS, Cialic R, Lanser AJ, Gabriely G, Koeglsperger T, Dake B, Wu PM, Doykan CE, Fanek Z, Liu L, Chen Z, Rothstein JD, Ransohoff RM, Gygi SP, Antel JP, Weiner HL (2014) Identification of a unique TGF-beta-dependent molecular and functional signature in microglia. Nat Neurosci 17:131–143. CrossRef Medline

Cavus I, Kasoff WS, Cassaday MP, Jacob R, Gueorguieva R, Sherwin RS, Krystal JH, Spencer DD, Abi-Saab WM (2005) Extracellular metabolites in the cortex and hippocampus of epileptic patients. Ann Neurol 57:226–235. CrossRef Medline

Davalos D, Grutzendler J, Yang G, Kim JV, Zuo Y, Jung S, Littman DR, Dustin ML, Gan WB (2005) ATP mediates rapid microglial response to local brain injury in vivo. Nat Neurosci 8:752–758. CrossRef Medline

Davalos D, Ryu JK, Merlini M, Baeten KM, Le Moan N, Petersen MA, Deerinck TJ, Smirnoff DS, Bedard C, Hakozaki H, Gonias Murray S, Ling JB, Lassmann H, Degen JL, Ellisman MH, Akassoglou K (2012) Fibrinogen-induced perivascular microglial clustering is required for the development of axonal damage in neuroinflammation. Nat Commun 3:1227. CrossRef Medline

Dibaj P, Nadrigny F, Steffens H, Scheller A, Hirrlinger J, Schomburg ED, Neusch C, Kirchhoff F (2010) NO mediates microglial response to acute spinal cord injury under ATP control in vivo. Glia 58:1133–1144. CrossRef Medline

Drage MG, Holmes GL, Seyfried TN (2002) Hippocampal neurons and glia in epileptic EL mice. J Neurocytol 31:681–692. CrossRef Medline

During MJ, Spencer DD (1993) Extracellular hippocampal glutamate and spontaneous seizure in the conscious human brain. Lancet 341:1607–1610. CrossRef Medline

Eyo U, Dailey ME (2012) Effects of oxygen-glucose deprivation on microglial mobility and viability in developing mouse hippocampal tissues. Glia 60:1747–1760. CrossRef Medline

Eyo UB, Dailey ME (2013) Microglia: key elements in neural development, plasticity, and pathology. J Neuroimmune Pharmacol 8:494–509. CrossRef Medline

Eyo UB, Wu LJ (2013) Bi-directional microglia-neuron communication in the healthy brain. Neural Plast 2013:456857. CrossRef Medline

Färber K, Markworth S, Pannasch U, Nolte C, Prinz V, Kronenberg G, Gertz K, Endres M, Bechmann I, Enjyoji K, Robson SC, Kettenmann H (2008) The ectonucleotidase cd39/ENTPDase1 modulates purinergic-mediated microglial migration. Glia 56:331–341. CrossRef Medline

Feng G, Mellor RH, Bernstein M, Keller-Peck C, Nguyen QT, Wallace M, Nerbonne JM, Lichtman JW, Sanes JR (2000) Imaging neuronal subsets in transgenic mice expressing multiple spectral variants of GFP. Neuron 28:41–51. CrossRef Medline

Fisher RS, van Emde Boas W, Blume W, Elger C, Genton P, Lee P, Engel J Jr (2005) Epileptic seizures and epilepsy: definitions proposed by the International League Against Epilepsy (ILAE) and the International Bureau for Epilepsy (IBE). Epilepsia 46:470–472. CrossRef Medline

Fontainhas AM, Wang M, Liang KJ, Chen S, Mettu P, Damani M, Fariss RN, Li W, Wong WT (2011) Microglial morphology and dynamic behavior is regulated by ionotropic glutamatergic and GABAergic neurotransmission. PLoS One 6:e15973. CrossRef Medline

Haynes SE, Hollopeter G, Yang G, Kurpius D, Dailey ME, Gan WB, Julius D (2006) The P2Y12 receptor regulates microglial activation by extracellular nucleotides. Nat Neurosci 9:1512–1519. CrossRef Medline

Hines DJ, Hines RM, Mulligan SJ, Macvicar BA (2009) Microglia processes block the spread of damage in the brain and require functional chloride channels. Glia 57:1610–1618. CrossRef Medline

Huang YJ, Maruyama Y, Dvoryanchikov G, Pereira E, Chaudhari N, Roper SD (2007) The role of pannexin 1 hemichannels in ATP release and cell-cell communication in mouse taste buds. Proc Natl Acad Sci U S A 104:6436–6441. CrossRef Medline

Jung S, Aliberti J, Graemmel P, Sunshine MJ, Kreutzberg GW, Sher A, Littman DR (2000) Analysis of fractalkine receptor CX(3)CR1 function by targeted deletion and green fluorescent protein reporter gene insertion. Mol Cell Biol 20:4106–4114. CrossRef Medline

Kaindl AM, Degos V, Peineau S, Gouadon E, Chhor V, Loron G, Le Charpentier T, Josserand J, Ali C, Vivien D, Collingridge GL, Lombet A, Issa L, Rene F, Loeffler JP, Kavelaars A, Verney C, Mantz J, Gressens P (2012) Activation of microglial N-methyl-D-aspartate receptors triggers inflammation and neuronal cell death in the developing and mature brain. Ann Neurol 72:536–549. CrossRef Medline

Kang J, Kang N, Lovatt D, Torres A, Zhao Z, Lin J, Nedergaard M (2008) Connexin 43 hemichannels are permeable to ATP. J Neurosci 28:4702–4711. CrossRef Medline

Kobayashi K, Yamanaka H, Fukuoka T, Dai Y, Obata K, Noguchi K (2008) P2Y12 receptor upregulation in activated microglia is a gateway of p38 signaling and neuropathic pain. J Neurosci 28:2892–2902. CrossRef Medline

Kuhn B, Denk W, Bruno RM (2008) In vivo two-photon voltage-sensitive dye imaging reveals top-down control of cortical layers 1 and 2 during wakefulness. Proc Natl Acad Sci U S A 105:7588–7593. CrossRef Medline

Kurtenbach S, Prochnow N, Kurtenbach S, Klooster J, Zoidl C, Dermietzel R, Kamermans M, Zoidl G (2013) Pannexin1 channel proteins in the zebrafish retina have shared and unique properties. PLoS One 8:e77722. CrossRef Medline

Liang KJ, Lee JE, Wang YD, Ma W, Fontainhas AM, Fariss RN, Wong WT (2009) Regulation of dynamic behavior of retinal microglia by CX3CR1 signaling. Invest Ophthalmol Vis Sci 50:4444–4451. CrossRef Medline

Li Y, Du XF, Liu CS, Wen ZL, Du JL (2012) Reciprocal regulation between resting microglial dynamics and neuronal activity in vivo. Dev Cell 23: 1189–1202. CrossRef Medline

Liu GJ, Nagarajah R, Banati RB, Bennett MR (2009) Glutamate induces directed chemotaxis of microglia. Eur J Neurosci 29:1108–1118. CrossRef Medline

Locovei S, Wang J, Dahl G (2006) Activation of pannexin 1 channels by ATP through P2Y receptors and by cytoplasmic calcium. FEBS Lett 580:239–244. CrossRef Medline

MacVicar BA, Thompson RJ (2010) Non-junction functions of pannexin-1 channels. Trends Neurosci 33:93–102. CrossRef Medline

Marín-Teva JL, Dusart I, Colin C, Gervais A, van Rooijen N, Mallat M (2004) Microglia promote the death of developing Purkinje cells. Neuron 41: 535–547. CrossRef Medline

Meurs A, Clinckers R, Ebinger G, Michotte Y, Smolders I (2008) Seizure activity and changes in hippocampal extracellular glutamate, GABA, dopamine and serotonin. Epilepsy Res 78:50–59. CrossRef Medline

Murugan M, Sivakumar V, Lu J, Ling EA, Kaur C (2011) Expression of N-methyl D-aspartate receptor subunits in amoeboid microglia mediates production of nitric oxide via NF-kappaB signaling pathway and oligodendrocyte cell death in hypoxic postnatal rats. Glia 59:521–539. CrossRef Medline

Nimmerjahn A, Kirchhoff F, Helmchen F (2005) Resting microglial cells are highly dynamic surveillants of brain parenchyma in vivo. Science 308: 1314–1318. CrossRef Medline

Ohsawa K, Sanagi T, Nakamura Y, Suzuki E, Inoue K, Kohsaka S (2012) Adenosine A3 receptor is involved in ADP-induced microglial process extension and migration. J Neurochem 121:217–227. CrossRef Medline

Orellana JA, Montero TD, von Bernhardi R (2013) Astrocytes inhibit nitric oxide-dependent Ca(2+) dynamics in activated microglia: involvement of ATP released via pannexin 1 channels. Glia 61:2023–2037. CrossRef Medline

Paolicelli RC, Bolasco G, Pagani F, Maggi L, Scianni M, Panzanelli P, Giustetto M, Ferreira TA, Guiducci E, Dumas L, Ragozzino D, Gross CT (2011) Synaptic pruning by microglia is necessary for normal brain development. Science 333:1456–1458. CrossRef Medline

Pascual O, Ben Achour S, Rostaing P, Triller A, Bessis A (2012) Microglia activation triggers astrocyte-mediated modulation of excitatory neurotransmission. Proc Natl Acad Sci U S A 109:E197–205. CrossRef Medline

Racine RJ (1972) Modification of seizure activity by electrical stimulation. II. Motor seizure. Electroencephalogr Clin Neurophysiol 32:281–294. CrossRef Medline

Ransohoff RM, Perry VH (2009) Microglial physiology: unique stimuli, specialized responses. Annu Rev Immunol 27:119–145. CrossRef Medline

Sasaki Y, Hoshi M, Akazawa C, Nakamura Y, Tsuzuki H, Inoue K, Kohsaka S (2003) Selective expression of Gi/o-coupled ATP receptor P2Y12 in microglia in rat brain. Glia 44:242–250. CrossRef Medline

Schafer DP, Lehrman EK, Stevens B (2013) The "quad-partite" synapse: microglia-synapse interactions in the developing and mature CNS. Glia 61:24–36. CrossRef Medline

Schafer DP, Lehrman EK, Kautzman AG, Koyama R, Mardinly AR, Yamasaki R, Ransohoff RM, Greenberg ME, Barres BA, Stevens B (2012) Microglia sculpt postnatal neural circuits in an activity and complement-dependent manner. Neuron 74:691–6705. CrossRef Medline

Shapiro LA, Wang L, Ribak CE (2008) Rapid astrocyte and microglial activation following pilocarpine-induced seizures in rats. Epilepsia 49 [Suppl 2]:33–41. CrossRef Medline

Sieger D, Moritz C, Ziegenhals T, Prykhozhij S, Peri F (2012) Long-range Ca2+ waves transmit brain-damage signals to microglia. Dev Cell 22: 1138–1148. CrossRef Medline

Thompson RJ, Jackson MF, Olah ME, Rungta RL, Hines DJ, Beazely MA, MacDonald JF, MacVicar BA (2008) Activation of pannexin-1 hemichannels augments aberrant bursting in the hippocampus. Science 322: 1555–1559. CrossRef Medline

Tozaki-Saitoh H, Tsuda M, Miyata H, Ueda K, Kohsaka S, Inoue K (2008) P2Y12 receptors in spinal microglia are required for neuropathic pain after peripheral nerve injury. J Neurosci 28:4949–4956. CrossRef Medline

Tremblay MÉ, Lowery RL, Majewska AK (2010) Microglial interactions with synapses are modulated by visual experience. PLoS Biol 8:e1000527. CrossRef Medline

Tzingounis AV, Wadiche JI (2007) Glutamate transporters: confining runaway excitation by shaping synaptic transmission. Nat Rev Neurosci 8:935–947. CrossRef Medline

Ueda Y, Doi T, Tokumaru J, Yokoyama H, Nakajima A, Mitsuyama Y, Ohya-Nishiguchi H, Kamada H, Willmore LJ (2001) Collapse of extracellular glutamate regulation during epileptogenesis: down-regulation and functional failure of glutamate transporter function in rats with chronic seizures induced by kainic acid. J Neurochem 76:892–900. Medline

Ueno M, Fujita Y, Tanaka T, Nakamura Y, Kikuta J, Ishii M, Yamashita T (2013) Layer V cortical neurons require microglial support for survival during postnatal development. Nat Neurosci 16:543–551. CrossRef Medline

Vezzani A, French J, Bartfai T, Baram TZ (2011) The role of inflammation in epilepsy. Nat Rev Neurol 7:31–40. CrossRef Medline

Vinet J, Weering HR, Heinrich A, Kälin RE, Wegner A, Brouwer N, Heppner FL, Rooijen Nv, Boddeke HW, Biber K (2012) Neuroprotective function for ramified microglia in hippocampal excitotoxicity. J Neuroinflammation 9:27. CrossRef Medline

Wake H, Moorhouse AJ, Jinno S, Kohsaka S, Nabekura J (2009) Resting microglia directly monitor the functional state of synapses in vivo and determine the fate of ischemic terminals. J Neurosci 29:3974–3980. CrossRef Medline

Wu LJ, Zhuo M (2008) Resting microglial motility is independent of synaptic plasticity in mammalian brain. J Neurophysiol 99:2026–2032. CrossRef Medline

Wu LJ, Vadakkan KI, Zhuo M (2007) ATP-induced chemotaxis of microglial processes requires P2Y receptor-activated initiation of outward potassium currents. Glia 55:810–821. CrossRef Medline

Wu LJ, Wu G, Akhavan Sharif MR, Baker A, Jia Y, Fahey FH, Luo HR, Feener EP, Clapham DE (2012) The voltage-gated proton channel Hv1 enhances brain damage from ischemic stroke. Nat Neurosci 15:565–573. CrossRef Medline